International Journal of Engineering, Mathematical and Physical Sciences
ISSN: 2517-9934
Vol:7, No:2, 2013

Equatorial Symmetry of Chaotic Solutions in Boussinesq Convection in a Rotating Spherical Shell

Keiji Kimura, Shin-ichi Takehiro, and Michio Yamada

Abstract—We investigate properties of convective solutions of the Boussinesq thermal convection in a moderately rotating spherical shell allowing the inner and outer sphere rotation due to the viscous torque of the fluid. The ratio of the inner and outer radii of the spheres, the Prandtl number and the Taylor number are fixed to 0.4, 1 and 500^2, respectively. The inertial moments of the inner and outer spheres are fixed to about 0.22 and 100, respectively. The Rayleigh number is varied from 2.6×10^4 to 3.4×10^4. In this parameter range, convective solutions transit from equatorially symmetric quasi-periodic ones to equatorially asymmetric chaotic ones as the Rayleigh number is increased. The transition route in the system allowing rotation of both the spheres is different from that in the co-rotating system, which means the inner and outer spheres rotate with the same constant angular velocity: the convective solutions transit as equatorially symmetric quasi-periodic solution $\rightarrow$ equatorially symmetric chaotic solution $\rightarrow$ equatorially asymmetric chaotic solution in the system allowing both the spheres rotation, while equatorially symmetric quasi-periodic solution $\rightarrow$ equatorially asymmetric quasi-periodic solution $\rightarrow$ equatorially asymmetric chaotic solution in the co-rotating system.

Keywords—thermal convection, numerical simulation, equatorial symmetry, quasi-periodic solution, chaotic solution

I. Introduction

THE problem of Boussinesq thermal convection in rotating spheres and spherical shells has been investigated vigorously for over half a century, not only as a fundamental model of the global thermal convection in stellar and planetary atmospheres and fluid cores but also as a purely fluid dynamics problem. There have been many researches to investigate behaviour of the solutions in this system theoretically and numerically since the pioneering work by Chandrasekhar [1].

Thanks to recent remarkable progress of computational ability, routes from critical modes to turbulent solutions with increasing the Rayleigh number are gradually revealed in some parameter ranges [2], [3], [4], [5]. When the Prandtl number is $O(1)$, as the Rayleigh number is increased, convective solutions transit as follows: a traveling wave solution, vacillating solution, quasi-periodic solution and chaotic solution [2]. As the Rayleigh number is further increased, localized turbulent convection pattern and the relaxation oscillation appear [4]. When the Prandtl number is relatively small $(O(10^{-1}))$, the spiralling columnar convection emerging as a critical mode in rapidly rotating cases becomes unstable at a larger Rayleigh number, and the amplitude vacillations, shape vacillations and the chaotic behaviours occur, and the relaxation oscillation occurs as the Rayleigh number is further increased [5]. When the Prandtl number is small $(O(10^{-2}))$, the equatorially attached convection pattern, which emerges as a critical mode, becomes modulate but is still concentrated near the outer sphere at a larger Rayleigh number. As the Rayleigh number is further increased, the equatorially attached eddies spread into interior region and become detached in some cases [5].

However, there have been few detailed researches around an emerging point of equatorially asymmetric convection patterns. Especially the route from equatorially symmetric pattern to equatorially asymmetric pattern, which is necessary for understanding a mechanism for emerging equatorially asymmetric pattern, is not well known. Then, in the present paper, we focus on the route from equatorially symmetric pattern to equatorially asymmetric one, and investigate the effect of the inner and outer spheres rotation on this route.

Actually, almost previous studies of thermal convection in rotating spherical shells so far have assumed that the inner and outer spheres rotate with the same constant angular velocity (co-rotation), possibly due to simplification of the configuration of the problem, while there are some magneto-hydrodynamic (MHD) dynamo models which permit the axial differential rotation of the inner sphere [6], [7]. However, the spheres do not necessary co-rotate in the actual astronomical bodies, and it is a more natural set up that both the spheres rotate freely. Actually, recent seismological researches suggest that the Earth's inner core differentially rotates with respect to the mantle in this decade [8], [9].

The model, governing equations and numerical methods are described in Sec. II. In Sec. III, we investigate the transition routes from equatorially symmetric convective solutions to equatorially asymmetric ones both in the system allowing rotation of both the spheres and in the co-rotating system, and also show some typical convection patterns. The conclusions and discussions are described in Sec. IV.

II. Model and numerical method

Let us consider a Boussinesq fluid in a spherical shell whose radii of the inner and outer spheres are $r_{\rm in}$ and $r_{\rm out}$, respectively. The inner and outer spheres rotate with $\tilde{\mathbf{\Omega}}_{\rm in}$ and $\tilde{\mathbf{\Omega}}_{\rm out}$, respectively, in the rotating frame of reference

Keiji Kimura is with Research Institute for Mathematical Sciences, Kyoto University, Kitashirakawa Oiwake-cho, Sakyo-ku, Kyoto 606-8502, Japan (phone: +81-75-753-7278, fax: +81-75-753-7272, e-mail: kimura@kurims.kyoto-u.ac.jp)

Shin-ichi Takehiro is with Research Institute for Mathematical Sciences, Kyoto University, Kitashirakawa Oiwake-cho, Sakyo-ku, Kyoto 606-8502, Japan (phone: +81-75-753-7260, fax: +81-75-753-7272, e-mail: takepiro@gfd-dennou.org)

Michio Yamada is with Research Institute for Mathematical Sciences, Kyoto University, Kitashirakawa Oiwake-cho, Sakyo-ku, Kyoto 606-8502, Japan (phone: +81-75-753-7221, fax: +81-75-753-7272, e-mail: yamada@kurims.kyoto-u.ac.jp)

with constant angular velocity $\Omega\boldsymbol{k}$. These mean that the inner and outer spheres rotate with $\tilde{\boldsymbol{\Omega}}_{\rm in} + \Omega\boldsymbol{k}$ and $\tilde{\boldsymbol{\Omega}}_{\rm out} + \Omega\boldsymbol{k}$, respectively, in the inertial frame of reference. Since the uniform heat source H per unit mass is distributed in the whole spherical shell region, the temperature distribution of the basic conductive state $T_s(r)$ is $T_s(r) = -\beta r^2/2 + T_0$, where $\beta \equiv H/(3\kappa C_p)$, κ is the thermal diffusivity, C_p the specific heat capacity, T_0 a constant. We consider the self-gravitational field of homogeneous media whose density is ρ, that is, $\boldsymbol{g} = -\gamma\boldsymbol{r}$, where $\gamma \equiv 4\pi G\rho/3$ is a constant (G is the universal gravitational constant) and $\boldsymbol{r}$ the position vector with respect to the center of the shell.

We choose the thickness of the shell $d \equiv r_{\rm out} - r_{\rm in}$ as the length scale, the viscous dissipation time d^2/ν as the time scale, and $\nu^2/(\gamma\alpha d^4)$ as the temperature scale, where ν is the kinematic viscosity and α the thermal expansion coefficient. The pressure is normalized with $\rho\nu^2/d^2$, and the inertial moments of the inner and outer spheres are done with ρd^5. The non-dimensional governing equations for the deviations from the conductive rest state in the rotating frame of reference with the angular velocity $\Omega\boldsymbol{k}$ are as follows:

$$\nabla \cdot \boldsymbol{U} = 0, \tag{1}$$

$$\frac{\partial \boldsymbol{U}}{\partial t} + (\boldsymbol{U}\cdot\nabla)\boldsymbol{U} + \tau\boldsymbol{k}\times\boldsymbol{U} = -\nabla\pi + \Theta\boldsymbol{r} + \Delta\boldsymbol{U}, \tag{2}$$

$$P\left(\frac{\partial\Theta}{\partial t} + (\boldsymbol{U}\cdot\nabla)\Theta\right) = R\,\boldsymbol{U}\cdot\boldsymbol{r} + \nabla^2\Theta, \tag{3}$$

where $\boldsymbol{U}$ is the non-dimensional velocity, π is the non-dimensional pressure, and Θ is the temperature deviation from the basic conductive state $T_s(r)$. The equations of motion of the inner and outer spheres are as follows:

$$I_{\rm in}\frac{d\tilde{\boldsymbol{\Omega}}_{\rm in}}{dt} = \boldsymbol{N}_{\rm in}(\boldsymbol{U}), \tag{4}$$

$$I_{\rm out}\frac{d\tilde{\boldsymbol{\Omega}}_{\rm out}}{dt} = \boldsymbol{N}_{\rm out}(\boldsymbol{U}), \tag{5}$$

where $I_{\rm in}$ and $I_{\rm out}$ are the non-dimensional inertial moments of the inner and outer spheres, respectively, and $\boldsymbol{N}_{\rm in}$ and $\boldsymbol{N}_{\rm out}$ are the non-dimensional torques on the inner and outer spheres. Here we assume that the centers of the spheres always keep the same position. The non-dimensional control parameters in the equations are

$$\eta = \frac{r_{\rm in}}{r_{\rm out}},\quad \tau = \sqrt{T} = \frac{2\Omega d^2}{\nu},\quad P = \frac{\nu}{\kappa},$$
$$R = \frac{\alpha\beta\gamma d^6}{\nu\kappa},\quad I_{\rm in} = \frac{I^*_{\rm in}}{\rho d^5},\quad I_{\rm out} = \frac{I^*_{\rm out}}{\rho d^5},$$

where η is the ratio of the radii of the inner and outer spheres, T the Taylor number, P the Prandtl number, and R the Rayleigh number. $I^*_{\rm in}$ and $I^*_{\rm out}$ mean the dimensional inertial moments of the inner and outer spheres, respectively.

We choose the boundary condition of the velocity as no-slip and impermeable on both spheres, and the temperature disturbance is fixed to zero at the inner and outer spheres:

$$\boldsymbol{U}(r = r_{\rm in}, \theta, \phi, t) = \tilde{\boldsymbol{\Omega}}_{\rm in}\times(r_{\rm in}\boldsymbol{e}_r), \tag{6}$$

$$\boldsymbol{U}(r = r_{\rm out}, \theta, \phi, t) = \tilde{\boldsymbol{\Omega}}_{\rm out}\times(r_{\rm out}\boldsymbol{e}_r), \tag{7}$$

$$\Theta(r = r_{\rm in}, \theta, \phi, t) = 0, \tag{8}$$

$$\Theta(r = r_{\rm out}, \theta, \phi, t) = 0, \tag{9}$$

where r is the radial distance from the origin, θ and ϕ are the zenith (colatitude) and the azimuth (longitude) with respect to the rotation axis, respectively, and $\boldsymbol{e}_r$ is the unit vector in the radial direction, and hereafter we use the spherical coordinate system.

Since the velocity field is solenoidal, it can be represented with the toroidal and poloidal potentials w and v as follows:

$$\boldsymbol{U} \equiv \nabla\times(\boldsymbol{r}(w + w_S)) + \nabla\times\{\nabla\times(\boldsymbol{r}v)\}, \tag{10}$$

where w_S is defined as

$$\begin{aligned} w_S(\boldsymbol{r}, \tilde{\boldsymbol{\Omega}}_{\rm in}(t), \tilde{\boldsymbol{\Omega}}_{\rm out}(t)) \\ \equiv -\frac{r_{\rm in}^3}{r_{\rm out}^3 - r_{\rm in}^3}\left(r - \frac{r_{\rm out}^3}{r^2}\right)\left(\boldsymbol{e}_r\cdot\tilde{\boldsymbol{\Omega}}_{\rm in}(t)\right) \\ + \frac{r_{\rm out}^3}{r_{\rm out}^3 - r_{\rm in}^3}\left(r - \frac{r_{\rm in}^3}{r^2}\right)\left(\boldsymbol{e}_r\cdot\tilde{\boldsymbol{\Omega}}_{\rm out}(t)\right), \end{aligned} \tag{11}$$

which satisfies the above velocity boundary conditions (6) and (7) [11]. Then the boundary conditions of v and w are

$$v = \frac{\partial v}{\partial r} = w = 0 \quad \text{at} \quad r = r_{\rm in},\ r_{\rm out}. \tag{12}$$

The governing equations of these potentials and Θ become

$$\begin{aligned} \frac{\partial}{\partial t}\left(\hat{L}_2 w\right) = \left[\nabla^2\hat{L}_2 + \tau\frac{\partial}{\partial\phi}\right]w - \tau\hat{Q}v \\ + \left[\left(\nabla^2 - \frac{\partial}{\partial t}\right)\hat{L}_2 + \tau\frac{\partial}{\partial\phi}\right]w_S \\ - \boldsymbol{r}\cdot\left[\nabla\times((\boldsymbol{U}\cdot\nabla)\boldsymbol{U})\right], \end{aligned} \tag{13}$$

$$\begin{aligned} \frac{\partial}{\partial t}\left(\hat{L}_2\nabla^2 v\right) = \left[\nabla^2\hat{L}_2 + \tau\frac{\partial}{\partial\phi}\right]\nabla^2 v + \tau\hat{Q}w - \hat{L}_2\Theta \\ + \tau\hat{Q}w_S \\ - \boldsymbol{r}\cdot\left[\nabla\times\nabla\times((\boldsymbol{U}\cdot\nabla)\boldsymbol{U})\right], \end{aligned} \tag{14}$$

$$P\frac{\partial\Theta}{\partial t} = R\hat{L}_2 v + \nabla^2\Theta - P(\boldsymbol{U}\cdot\nabla)\Theta, \tag{15}$$

where $\hat{L}_2$ and $\hat{Q}$ are the operators defined as

$$\hat{L}_2 \equiv -\frac{1}{\sin^2\theta}\left[\sin\theta\frac{\partial}{\partial\theta}\left(\sin\theta\frac{\partial}{\partial\theta}\right) + \frac{\partial^2}{\partial\phi^2}\right], \tag{16}$$

$$\hat{Q} \equiv \boldsymbol{k}\cdot\nabla - \frac{1}{2}\left[\hat{L}_2(\boldsymbol{k}\cdot\nabla) + (\boldsymbol{k}\cdot\nabla)\hat{L}_2\right]. \tag{17}$$

We will fix the values of η and P as the standard values $\eta = 0.4$ and $P = 1$, and also fix τ as 500, which means the moderately rotating region, and vary the Rayleigh number in the range of $2.6\times10^4 \le R \le 3.4\times10^4$. The inertial moment of the inner sphere is set to be $I_{\rm in} = 8\pi r_{\rm in}^5/15 \simeq 0.22$, assuming that the density of the inner sphere is the same as that of fluid. This assumption is consistent with the self-gravitational field. The inertial moment of the outer sphere is set to be $I_{\rm out} = 100$, which is the simulated non-dimensional value of the inertial

moment of the Earth's mantle when the inner sphere and the shell are considered to be the inner core and the outer core of the Earth, respectively.

The Galerkin-spectral method is applied to the toroidal and poloidal potentials and the temperature disturbance. They are expanded with the spherical harmonics in the horizontal (azimuthal and zenith) directions, and with the combinations of Chebyshev polynomials which satisfy the boundary conditions in the radial direction (8), (9) and (12) [12]. We also use the Crank-Nicolson scheme to the diffusion terms and use the second order Adams-Bashforth scheme for all other terms, with the time step 10^{-4}. The truncation wavenumber of spherical harmonics and the maximum degree of the Chebyshev polynomials are set to both fixed to 42. The nonlinear terms in the governing equations are evaluated in the physical space and are converted back into the spectral space (the spectral transform method). The numbers of the grid points on the physical space are chosen as $(N_r, N_\theta, N_\phi) = (65, 64, 128)$ in order to eliminate the aliasing errors, where N_r, N_θ and N_ϕ the number of grid points in the radial, zenith (colatitudinal) and azimuthal (longitudinal) directions, respectively. At the initial state, both the spheres do not rotate in the rotating frame of reference with constant angular velocity $\Omega \boldsymbol{k}$, and the random temperature disturbance is added to the conductive state.

III. Results

A. Transition diagram

In our parameter range, as the Rayleigh number is increased, the convective solutions with equatorial symmetry transit to those with equatorial asymmetry. We should remark the definition of the equatorial symmetry, antisymmetry and asymmetry of the convective solutions. The equatorially symmetric (antisymmetric) part of convective solution $(\boldsymbol{U}, \Theta)$ satisfied the following relations with the upper (lower) signature:

$$\begin{aligned} U_r(r,\theta,\phi) &= \pm U_r(r,\pi-\theta,\phi), \\ U_\theta(r,\theta,\phi) &= \mp U_\theta(r,\pi-\theta,\phi), \\ U_\phi(r,\theta,\phi) &= \pm U_\phi(r,\pi-\theta,\phi), \\ \Theta(r,\theta,\phi) &= \pm \Theta(r,\pi-\theta,\phi). \end{aligned}$$

When the convective solution consists of only equatorially symmetric part we call this as equatorially symmetric solution and when that consists of both equatorially symmetric and antisymmetric parts we call this as equatorially asymmetric solution.

Figure 1 shows the transition diagram of these convective solutions in the range $2.7\times10^4 \le R \le 3.2\times10^4$. $\mathrm{QP^S}$ means a quasi-periodic (or periodic) solution with equatorial symmetry, $\mathrm{QP^A}$ a quasi-periodic (or periodic) solution with equatorial asymmetry, $\mathrm{C^S}$ a chaotic solution with equatorial symmetry, and $\mathrm{C^S}$ a chaotic solution with equatorial asymmetry. In the system allowing rotation of both the spheres, the convective solutions transit as $\mathrm{QP^S} \to \mathrm{C^S} \to \mathrm{C^A}$, as the Rayleigh number is increased. However, in the co-rotating system, the convective solutions transit as $\mathrm{QP^S} \to \mathrm{QP^A} \to \mathrm{C^A}$, as the Rayleigh number is increased. Moreover, the chaotic solutions appear at lower Rayleigh number in the system allowing rotation of both the spheres comparing with that in the co-rotating system. In the system allowing rotation of only the inner sphere ($\tilde{\boldsymbol{\Omega}}_{\mathrm{out}} = \boldsymbol{0}$), the transition diagram from equatorially symmetric convective solutions to equatorially asymmetric ones is exactly same as that in the system allowing rotation of both the spheres. Therefore we conclude that the inner sphere free rotation causes the change of transition route from equatorially symmetric convective solutions to equatorially asymmetric ones and also does the appearance of chaotic solutions at lower Rayleigh number.

B. Typical behaviors of $\mathrm{QP^S}$, $\mathrm{C^S}$ and $\mathrm{C^A}$

In this section we show some typical behaviours of the convective solutions. In the system allowing rotation of both the spheres, $\mathrm{QP^S}$ solution appears at $R = 2.6\times10^4$, $\mathrm{C^S}$ at $R = 3.0\times10^4$, and $\mathrm{C^A}$ at $R = 3.4\times10^4$, while $\mathrm{QP^S}$ solution appears at $R = 2.6\times10^4$, $\mathrm{QP^A}$ at $R = 3.0\times10^4$, and $\mathrm{C^A}$ at $R = 3.4\times10^4$ in the co-rotating system

Figure 2 shows the time series of the angular velocities of the inner and outer spheres of $\mathrm{QP^S}$ solution at $R = 2.6\times10^4$ and $\mathrm{C^S}$ at $R = 3.0\times10^4$. Because $\mathrm{QP^S}$ and $\mathrm{C^S}$ solutions have equatorial symmetry, the perpendicular components of the angular velocities of both the inner and outer spheres against the axis of rotation of reference are exactly zero, and the axial component of that of the inner sphere $\tilde{\Omega}_{\mathrm{in},z}$ and that of the outer sphere $\tilde{\Omega}_{\mathrm{out},z}$ are shown in Fig. 2.

When $R = 2.6\times10^4$ in the system allowing rotation of the spheres (left panel in Fig. 2), the inner sphere rotates in the retrograde direction with fluctuations: $\tilde{\Omega}_{\mathrm{in},z} = -7.0 \pm 1.5$. On the other hand the outer sphere rotates in the prograde direction with fluctuations: $\tilde{\Omega}_{\mathrm{out},z} = +0.42 \pm 0.017$. The magnitude of the inner sphere rotation is $\overline{\tilde{\Omega}_{\mathrm{in},z}}/\Omega \simeq 3\%$, where $\Omega = \tau/2 = 250$, while that of the outer sphere is $\overline{\tilde{\Omega}_{\mathrm{out},z}}/\Omega \simeq 0.2\%$, relatively smaller than that of the inner sphere because the inertial moment of the inner sphere is much smaller than that of the outer sphere in our parameter range ($I_{\mathrm{in}} \simeq 0.22 \ll I_{\mathrm{out}} = 100$). It is found that the dominant azimuthal wavenumber of this $\mathrm{QP^S}$ solution is 2: $\overline{E_k^{m=2}}/\overline{E_k} \simeq 63\%$. Here kinetic energy density for each azimuthal wavenumber m E_k^m is defined by

$$E_k^m \equiv \frac{1}{V_{\mathrm{shell}}} \int_{V_{\mathrm{shell}}} \frac{1}{2} |\boldsymbol{U}^m|^2 dV,$$

and $\boldsymbol{U}^m$ is the velocity for azimuthal wavenumber m. The total kinetic energy density E_k is defined by

$$\begin{aligned} E_k &\equiv \frac{1}{V_{\mathrm{shell}}} \int_{V_{\mathrm{shell}}} \frac{1}{2} |\boldsymbol{U}|^2 dV, \\ &= \sum_m E_k^m, \end{aligned}$$

because $\int_{V_{\mathrm{shell}}} \boldsymbol{U}^m \cdot \boldsymbol{U}^{m'} dV = 0$ for $m \neq m'$. The overline $\bar{\cdot}$ means the time averaged value. This $\mathrm{QP^S}$ solution propagates in the retrograde direction: $\overline{v_p} \simeq -2.0$.

The behaviour of $\mathrm{QP^S}$ solution at $R = 2.6\times10^4$ in the co-rotating system are qualitatively similar to that of $\mathrm{QP^S}$ solution in the system allowing rotation of both the spheres.

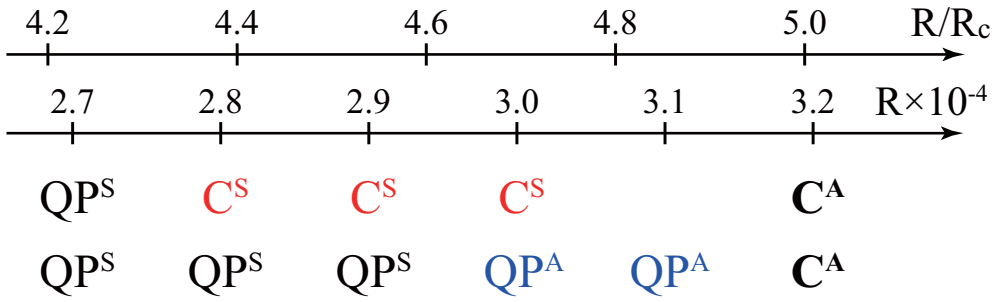

Fig. 1. Property of convective solution at each Rayleigh number. $\mathrm{QP^S}$: quasi-periodic (or periodic) solution with equatorial symmetry, $\mathrm{QP^A}$: quasi-periodic (or periodic) solution with equatorial asymmetry, $\mathrm{C^S}$: chaotic solution with equatorial symmetry, $\mathrm{C^S}$: chaotic solution with equatorial asymmetry. $R_c = 6387$ is the critical Rayleigh number. The upper row shows properties of convective solutions in the system allowing rotation of both the spheres, while the lower one shows those in the co-rotating system.

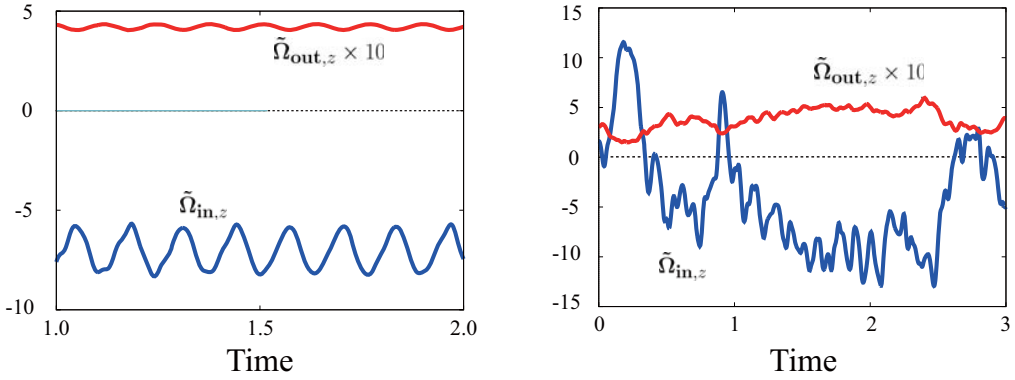

Fig. 2. Time series of the angular velocities of the inner and outer spheres of $\mathrm{QP^S}$ solution at $R = 2.6 \times 10^4$ (left) and those of $\mathrm{C^S}$ at $R = 3.0 \times 10^4$ (right) in the system allowing rotation of both the spheres. Blue solid line shows the axial component of the angular velocity of the inner sphere $\tilde{\Omega}_{\mathrm{in},z}$, and red solid line shows that of the outer sphere $\tilde{\Omega}_{\mathrm{out},z}$).

The dominant azimuthal wavenumber of $\mathrm{QP^S}$ solution in the co-rotating system is 2 and this propagates in the retrograde direction ($\overline{v_p} \simeq -1.5$).

The behaviour of $\mathrm{QP^A}$ solution at $R = 3.0 \times 10^4$ in the co-rotating system are also qualitatively similar to that of $\mathrm{QP^S}$ solution at $R = 2.6 \times 10^4$ in the co-rotating system. The dominant azimuthal wavenumber of $\mathrm{QP^S}$ solution in the co-rotating system is 2 and this propagates in the retrograde direction ($\overline{v_p} \simeq -2.1$). This is consistent with the fact that the antisymmetric part of kinetic energy density of $\mathrm{QP^A}$ solution is less than 1% of total kinetic energy density: $\overline{E_k^{\mathrm{Anti}}}/\overline{E_k^{\mathrm{S}}} \simeq 0.75\%$, where E_k^{S} and E_k^{Anti} are defined by

$$E_k^{\mathrm{S}} \equiv \frac{1}{V_{\mathrm{shell}}} \int_{V_{\mathrm{shell}}} \frac{1}{2} |\boldsymbol{U}^{\mathrm{S}}|^2 dV,$$
$$E_k^{\mathrm{Anti}} \equiv \frac{1}{V_{\mathrm{shell}}} \int_{V_{\mathrm{shell}}} \frac{1}{2} |\boldsymbol{U}^{\mathrm{Anti}}|^2 dV,$$

where $\boldsymbol{U}^{\mathrm{S}}$ and $\boldsymbol{U}^{\mathrm{Anti}}$ are the symmetric and antisymmetric part of the velocity, respectively.

As the Rayleigh number is increased up to $R = 3.0 \times 10^4$ in the system allowing rotation of the spheres, $\mathrm{C^S}$ convective solution appears, shown at right panel in Fig. 2. When $R = 3.0 \times 10^4$, the inner sphere averagely rotates in the retrograde direction ($\overline{\tilde{\Omega}_{\mathrm{in},z}} = -5.2$), but sometimes is accelerated to rotate in the prograde direction ($\tilde{\Omega}_{\mathrm{in},z} = +11.6$ at $t = 0.2$, for instance). The magnitude of the inner sphere rotation is at most 5.3%, larger than that of $\mathrm{QP^S}$ solution at $R = 2.6 \times 10^4$. On the other hand, the outer sphere keeps rotate in the prograde direction ($\overline{\tilde{\Omega}_{\mathrm{out},z}} = +0.40$), but sometimes is decelerated to be about $+0.2$ at $t = 0.2$, for instance. When $\tilde{\Omega}_{\mathrm{in},z} < 0$ the dominant azimuthal wavenumber is 2: $\overline{E_k^{m=2}}/\overline{E_k} \simeq 58\%$ at $t = 2.0$, and this tendency is similar to that of $\mathrm{QP^S}$ solution at $R = 2.6 \times 10^4$. However, when $\tilde{\Omega}_{\mathrm{in},z}$ is accelerated to become positive at $t = 0.2$, for instance, $\tilde{\Omega}_{\mathrm{out},z}$ is simultaneously decelerated, and at that time the dominant azimuthal wavenumber is not $m = 2$ but $m = 4$ and 5. These behaviours of $\mathrm{C^S}$ solution are very different from those of $\mathrm{QP^S}$ solution.

As the Rayleigh number is further increased up to $R = 3.4 \times 10^4$ in the system allowing rotation of the spheres, $\mathrm{C^A}$ convective solution appears, shown in Fig. 3. When $R = 3.4 \times 10^4$, the inner sphere averagely rotate in the retrograde direction ($\overline{\tilde{\Omega}_{\mathrm{in},z}} = -4.1$) but sometimes is accelerated to rotate in the prograde direction ($\tilde{\Omega}_{\mathrm{in},z} = +14.9$ at $t = 3.9$, for instance), similar to the behaviour of $\mathrm{C^S}$ solution at $R = 3.0 \times 10^4$. The magnitude of the inner sphere rotation is at

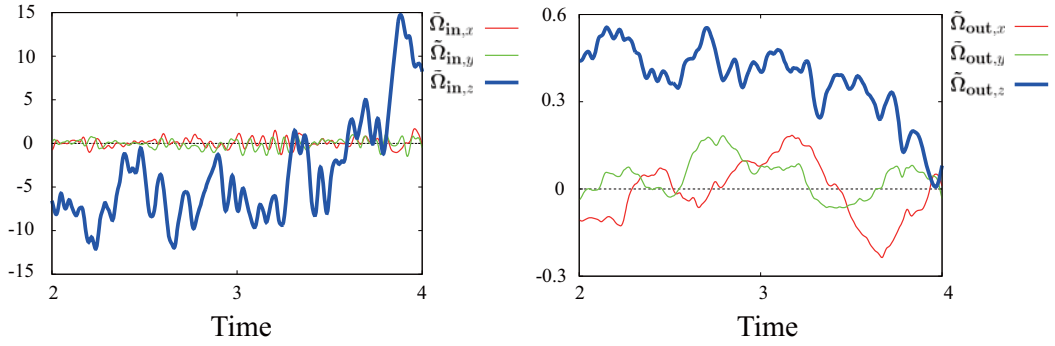

Fig. 3. Time series of the angular velocities of the inner (left) and outer (right) spheres, $\tilde{\mathbf{\Omega}}_{\mathrm{in}}$ and $\tilde{\mathbf{\Omega}}_{\mathrm{out}}$, of $\mathrm{C^A}$ solution at $R = 3.4 \times 10^4$ in the system allowing rotation of both the spheres.

most 5.9%, larger than that of $\mathrm{C^S}$ solution at $R = 3.0 \times 10^4$. The perpendicular components of $\tilde{\mathbf{\Omega}}_{\mathrm{in}}$ fluctuate around zero (the standard deviations of $\tilde{\Omega}_{\mathrm{in},x}$ and $\tilde{\Omega}_{\mathrm{in},y}$ are both about 0.5), and their magnitudes against $\tilde{\Omega}_{\mathrm{in},z}$ are relatively small: $|\tilde{\Omega}_{\mathrm{in},x}|/|\tilde{\Omega}_{\mathrm{in},z}| \simeq 11\%$ at $t = 3.0$. On the other hand, the outer sphere keeps rotate in the prograde direction ($\overline{\tilde{\Omega}_{\mathrm{in},z}} = +0.36$), but sometimes decelerated to be about $+0.01$ at $t = 3.9$, for example. The perpendicular components of $\tilde{\mathbf{\Omega}}_{\mathrm{out}}$ fluctuate around zero, and $|\tilde{\Omega}_{\mathrm{out},x}|/|\tilde{\Omega}_{\mathrm{out},z}| \simeq 20\%$ at $t = 3.0$, relatively larger than the ratio of the magnitude of $|\tilde{\Omega}_{\mathrm{in},x}|/|\tilde{\Omega}_{\mathrm{in},z}|$. When $\tilde{\Omega}_{\mathrm{in},z} < 0$ the dominant azimuthal wavenumber is 2, same as that of $\mathrm{QP^S}$ at $R = 2.6 \times 10^4$. On the other hand, when $\tilde{\Omega}_{\mathrm{in},z} > 0$ at $t = 3.9$, for instance, the dominant azimuthal wavenumber is not 2 but 4. The antisymmetric part of the kinetic energy density is smaller than the symmetric one: $\max(E_k^{\mathrm{Anti}})/E_k^{\mathrm{S}} \simeq 12\%$.

The behaviours of $\mathrm{C^A}$ in the co-rotating system are qualitatively similar to those of $\mathrm{C^A}$ in the system allowing rotation of the spheres.

IV. Conclusion and Discussion

We investigated the route from the equatorial symmetric pattern to the equatorial asymmetric pattern in the system allowing the rotation of both spheres and in the co-rotating system, under the impermeable, no-slip and fixed-temperature boundary conditions for the ratio of inner and outer radii of the shell $\eta = 0.4$, the Prandtl number $P = 1$, the rotation rate $\tau = 500$, the inertial moments of the inner and outer spheres $I_{\mathrm{in}} \simeq 0.22$ and $I_{\mathrm{out}} = 100$, respectively. We found that, as the Rayleigh number is increased in the range $2.6 \times 10^4 \leq R \leq 3.4 \times 10^4$, the convective solutions transit as $\mathrm{QP^S} \to \mathrm{C^S} \to \mathrm{C^A}$ in the system allowing rotation of both the spheres while those transit as $\mathrm{QP^S} \to \mathrm{QP^A} \to \mathrm{C^A}$ in the co-rotating system (Fig. 1). In the system allowing rotation of only the inner sphere ($\tilde{\mathbf{\Omega}}_{\mathrm{out}} = \mathbf{0}$), the transition diagram shown in Fig 1 is exactly same as that in the system allowing rotation of both the spheres. Therefore we conclude that the inner sphere free rotation causes the change of transition route from equatorially symmetric convective solutions to equatorially asymmetric ones.

When $R = 2.6 \times 10^4$ in the system allowing rotation of both the spheres, $\mathrm{QP^S}$ solution appears (shown at right panel in Fig. 2) and the inner sphere rotates in the retrograde direction while the outer sphere does in the prograde direction. The dominant azimuthal wavenumber is 2, which is smaller than the critical azimuthal wavenumber of the conductive state $m_c = 4$ [10]. As the Rayleigh number is increased up to $R = 3.0 \times 10^4$ $\mathrm{C^S}$ solution appears (left panel in Fig. 2): the inner sphere averagely rotates in the retrograde direction but sometimes is accelerated to be positive while the outer sphere keeps prograde rotation. When $\tilde{\Omega}_{\mathrm{in},z} < 0$ the behaviour of $\mathrm{C^S}$ is qualitatively similar to that of $\mathrm{QP^S}$ at $R = 2.6 \times 10^4$, but when $\tilde{\Omega}_{\mathrm{in},z} > 0$ the behaviour is totally different from that of $\mathrm{QP^S}$. The behaviour of $\mathrm{C^A}$ at $R = 3.4 \times 10^4$ (Fig. 3) is qualitatively similar to that of $\mathrm{C^S}$, because the amplitude of the antisymmetric part of $\mathrm{C^A}$ is small compared with that of the symmetric one.

We consider that $\mathrm{C^S}$ at $R = 3.0 \times 10^4$ wanders around the unstable $\mathrm{QP^S}$ but sometimes goes away from $\mathrm{QP^S}$. Further quantitative researches should be done. Also the reason for sudden acceleration of the inner sphere as well as the changes of the convective motion and the zonal flow structure should be investigated as a future work.

Acknowledgment

Numerical calculations were performed with the computer systems of the Institute for Information Management and Communication (IIMC) of Kyoto University and with the computer systems of Research Institute for Mathematical Sciences (RIMS), Kyoto University. For the calculations of the finite-amplitude convective solutions, we used the library for spectral transform 'ISPACK' (http://www.gfd-dennou.org/arch/ispack/) [13] and its Fortran90 wrapper library 'SPMODEL library' (http://www.gfd-dennou.org/library/spmodel/) [14]. The products of the Dennou Ruby project (http://www.gfd-dennou.org/library/ruby/) were used to draw the figures. This work was supported by a Grant in-Aid for the Global COE Program "Fostering top leaders in mathematics – broadening the core and exploring new ground" from the Ministry of Education, Culture, Sports, Science and Technology (MEXT) of Japan.

REFERENCES

[1] S. Chandrasekhar, "Hydrodynamic and Hydromagnetic stability," Oxford Univ. Press, pp654 (1961).
[2] M. Ardes, F. H. Busse and J. Wicht, "Thermal convection in rotating spherical shells," Physics of the Earth and Planetary Interiors, **99**, 55 (1997).
[3] A. Tilgner and F. H. Busse, "Finite-amplitude convection in rotating spherical fluid shells," J. Fluid Mech., **332**, 359 (1997).
[4] E. Grote and F. H. Busse, "Dynamics of convection and dynamos in rotating spherical fluid shells," Fluid Dynamics Research, **28**, 349 (2001).
[5] R. Simitev and F. H. Busse, "Patterns of convection in rotating spherical shells," New Journal of Physics, **5**, 97.1 (2003).
[6] G.A. Glatzmaier and P.H. Roberts, "A three-dimensional convective dynamo solution with rotating and finitely conducting inner core and mantle," Phys. Earth Planet. Inter., **91**, 63 (1995).
[7] U.R. Christensen, J. Aubert, P. Cardin, E. Dormy, S. Gibbons, G.A. Glatzmaier, E. Grote, Y. Honkura, C. Jones, M. Kono, M. Matsushima, A. Sakuraba, F. Takahashi, A. Tilgner, J. Wicht, K. Zhang, "A numerical dynamo benchmark," Phys. Earth Planet. Inter., **128**, 25 (2001).
[8] J. Tromp, "Inner-core anisotropy and rotation," Annu. Rev. Earth Planet. Sci, **29**, 47 (2001).
[9] J. Zhang, X. Song, Y. Li, P. G. Richards, X. Sun and F. Waldhauser, "Inner core differential motion confirmed by earthquake waveform doublets," Science, **309**, 1357 (2005).
[10] K. Kimura, S. Takehiro and M. Yamada, "Stability and a bifurcation diagram of Boussinesq thermal convection in a moderately rotating spherical shell allowing rotation of the inner sphere," (2013, submitted).
[11] L. D. Landau and E. M. Lifshitz, "Fluid Mechanics, Second edition: Volume 6 (Course of Theoretical Physics)," Butterworth-Heinemann (1987).
[12] K. Kimura, S. Takehiro and M. Yamada, "Stability and bifurcation diagram of Boussinesq thermal convection in a moderately rotating spherical shell," Phys. Fluids, **23**, 074101 (2011).
[13] K. Ishioka, ispack-0.96, http://www.gfd-dennou.org/arch/ispack/, GFD Dennou Club (2011).
[14] S. Takehiro, Y. Sasaki, Y. Morikawa, K. Ishioka, M. Odaka, Y.O. Takahashi, S. Nishizawa, K. Nakajima, M. Ishiwatari and Y.-Y. Hayashi, SPMODEL Development Group, Hierarchical Spectral Models for GFD (SPMODEL), http://www.gfd-dennou.org/library/spmodel/, GFD Dennou Club (2011).